Image Modeling Using Interscale Phase Properties of Complex Wavelet Coefficients

Mark Miller, *Member, IEEE*, and Nick Kingsbury, *Member, IEEE*

Abstract—This paper describes an approach to image modelling using interscale phase relationships of wavelet coefficients for use in image estimation applications. The method is based on the dual tree complex wavelet transform, but a phase rotation is applied to the coefficients to create complex "derotated" coefficients. These derotated coefficients are shown to have increased correlation compared to standard wavelet coefficients near edge and ridge features allowing improved signal estimation in these areas. The nature of the benefits brought by the derotated coefficients are analyzed and the implications for image estimation algorithm design noted. The observations and conclusions provide a basis for design of the denoising algorithm in [1].

Index Terms—Complex, denoising, derotated, derotation, estimation, image modeling, interscale, wavelet.

I. INTRODUCTION

W AVELET transforms have emerged as a popular basis for photographic image modeling and restoration, due to the statistically useful properties of wavelet coefficients of natural images. Methods of parameterizing image statistics, including those of neighborhoods of wavelet coefficients, often involve the use of covariance information [2]. Here, we examine the covariance information for groups of wavelet coefficients near discontinuities and show how using phase information from coefficients at the next coarser level has the potential to make covariance based estimation more effective. The multiscale transform used is the dual tree complex wavelet transform (DTCWT) [3], [4].

Interscale phase relationships of wavelet coefficients have previously been used in texture synthesis [5] and in object recognition [6]. Suggesting the use of interscale phase relationships in image quality measurement, Wang and Simoncelli [7] provide a good analysis of local phase near scale invariant features for a certain class of continuous wavelets consisting of a low-pass filter modulated with a complex exponential. Romberg *et al.* [8] discuss interscale phase relationships and the topic is closely related to Kovesi's use of phase congruence in edge detection [9], [10].

We focus on discontinuities, assuming initially that the neighborhood of wavelet coefficients considered is dominated by the presence of an edge or ridge,[1] i.e., any other features present have little effect on the wavelet coefficient magnitudes. A companion paper to this one [1] demonstrates the successful use of the proposed image modeling in a state-of-the-art denoising algorithm and shows how to combine the specific modeling of discontinuities with standard modeling using an adaptive Bayesian model section framework. A more accessible introduction to the use of interscale phase relationships in covariance based estimation is given in [11].

Section II gives background on the wavelet transform used here and on the phase characteristics of wavelet coefficients. Section III provides a theoretical framework that motivates the use of interscale phase relationships to improve signal estimation performance by using a representation with higher signal correlation. An approach to using interscale phase in estimation algorithms is recommended in Section IV proposing the use of a novel 'derotated' coefficient. Section IV also provides some examples to familiarize the reader with the coefficients in 2-D then illustrates the limitations of the method and states the implications for image estimation algorithm design. In Section V, we show that the greater phase alignment of derotated coefficients seen in Section IV does, indeed, translate to higher correlation between coefficients (which is not guaranteed) and examine the nature of the improvement.

II. BACKGROUND

A. Dual Tree Complex Wavelet Transform

The DTCWT uses a dual tree of real wavelet filters to generate the real and imaginary parts of complex wavelet coefficients. This introduces a limited amount of redundancy and allows the transform to provide approximate shift invariance and directionally selective filters, while preserving the usual properties of perfect reconstruction and computational efficiency.

For a d-dimensional input, an L scale DT-CWT outputs an array of real scaling coefficients corresponding to the lowpass subbands in each dimension and $(4^d - 2^d)/2$ directional subbands of $M/2^{dl}$ complex wavelet coefficients at level l, where $l = 1 \ldots L$ and M is the total size of the input data. The total redundancy of the transform is 2^d and independent of L. The mechanics of the DT-CWT are not covered here. See [3] and

[1]Note that the discontinuity need only be dominant at the scale and orientation of the neighborhood considered. For example, fine texture surrounding a multiscale discontinuity will not greatly disrupt the modeling at coarser levels.
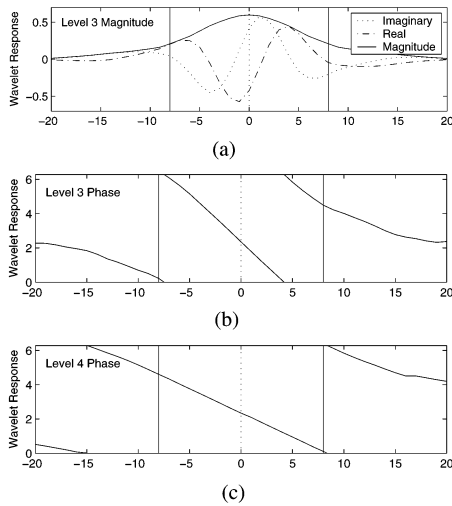
Fig. 1. Magnitude and phase response of a level 3 wavelet coefficient and phase response of a level 4 coefficient to a step input at a range of offsets. Adapted with permission from code used to generate graphics in [6]. (a) Magnitude response at level 3. (b) Phase response at level 3. (c) Phase response at level 4.
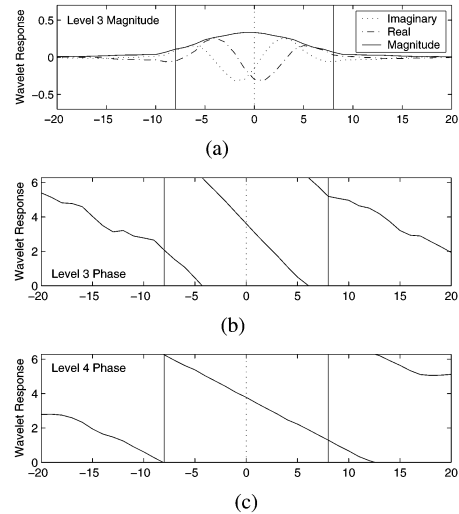

Fig. 2. Magnitude and phase response of a level 3 wavelet coefficient and phase response of a level 4 coefficient to an impulse input at a range of offsets. Adapted with permission from code used to generate graphics in [6]. (a) Magnitude response at level 3. (b) Phase response at level 3. (c) Phase response at level 4.

[4] for a comprehensive explanation of the transform and details of filter design for the trees.

In two dimensions, the transform produces six directional subbands at each scale. We will often refer to a local neighborhood of wavelet coefficients. This is defined as a group of coefficients at nearby spatial locations and adjacent scales. Parent and child coefficients refer to coefficients in the next coarser and finer subbands respectively in the same directional subband set and at the same spatial location (possibly interpolated).

B. Phase Characteristics of Complex Wavelet Coefficients

A well-known property of the Fourier transform is that a shift in the time or spatial domain corresponds to a linear phase ramp in the Fourier domain as shown in (1)

$$h(t - \alpha) \rightleftharpoons H(f)e^{-i2\pi\alpha f}. \tag{1}$$

Consider an input signal consisting of an object in the spatial or time domain. A shift of α will result in a phase shift of $2\pi\alpha f_0$ at frequency f_0 in the Fourier domain. A "moving" object will cause the Fourier coefficients to rotate at a rate proportional to their frequency f.

DT-CWT coefficients display similar properties to Fourier coefficients for small offsets of a dominant feature in the vicinity of the coefficient. DT-CWT subbands are centered on a frequency twice that of the next coarser level. Assume the presence of a single ridge or edge feature at a given scale, orientation and location. Because adjacent wavelet coefficients are at different locations relative to the feature, the phase of a complex coefficient will tend to be offset from its neighbor by an amount twice that of the corresponding parent coefficient (interpolated at the same location as the child), provided the feature is multiscale and the frequency spectrum of the feature behaves similarly across both of the scales.

This useful relationship is best illustrated in a 1-D setting. Fig. 1(a) shows the response of the magnitude and the real and imaginary parts for a level 3 DT-CWT coefficient as a 1-D step function is translated past it. Fig. 1(b) and (c) shows the phase

response of the coefficients at levels 3 and 4 to the same step. The horizontal axes give the translation of the step. Fig. 2 shows the same results for an impulse input. In both cases, the phase of the level 3 coefficient changes at approximately twice the rate of its parent at level 4.

III. CORRELATION AND SIGNAL ESTIMATION

In this section, we present a framework that motivates the use of interscale phase in image estimation applications. We examine the effect of signal correlation in Wiener estimation and show that for two Gaussian variables in additive Gaussian noise, estimation error decreases as the absolute value of the difference between the noise and signal correlation coefficients increases. This means that if the noise correlation magnitude is lower than that of the signal the error variance is a decreasing function of the signal correlation magnitude.

For a redundant transform like the DT-CWT, noise in the wavelet domain is not strictly uncorrelated. However, the correlation is generally significantly less than for the signal component. This leads to the conclusion that if a signal can be represented such that it displays additional correlation, e.g., using the relationships described in the previous section, signal estimation accuracy could be improved.

A. Effect of Signal Correlation in Wiener Filtering

Consider the estimation of a Gaussian variable from the observation of two correlated variables in Gaussian noise. We show that the Wiener estimation error as a function of the signal correlation coefficient is concave and has a local maximum where the value of the signal correlation coefficient is equal to that of the noise.

The framework used is the standard denoising problem but with only two variables

$$\mathbf{y} = \mathbf{x} + \mathbf{n}$$
$$\begin{bmatrix} y_1 \\ y_2 \end{bmatrix} = \begin{bmatrix} x_1 \\ x_2 \end{bmatrix} + \begin{bmatrix} n_1 \\ n_2 \end{bmatrix}.$$

$\mathbf{x}$ and $\mathbf{n}$ are zero mean and have covariance matrices $\mathbf{C_x}$ and $\mathbf{C_n}$, i.e., $\mathbf{x} \sim \mathcal{N}(0, \mathbf{C_x})$ and $\mathbf{n} \sim \mathcal{N}(0, \mathbf{C_n})$. $\mathbf{C_x}$ and $\mathbf{C_n}$ are parameterized as shown in (2) and (3). ρ_x and ρ_n are correlation coefficients and have values between negative one and one inclusive. Note that we exclude the cases where $|\rho_x| = |\rho_n| = 1$, since, in these cases, the observations are deterministically linked

$$\mathbf{C_x} = \begin{bmatrix} \sigma_x^2 & \rho_x \sigma_x^2 \\ \rho_x \sigma_x^2 & \sigma_x^2 \end{bmatrix} \tag{2}$$

$$\mathbf{C_n} = \begin{bmatrix} \sigma_n^2 & \rho_n \sigma_n^2 \\ \rho_n \sigma_n^2 & \sigma_n^2 \end{bmatrix}. \tag{3}$$

The standard Wiener estimate $\hat{\mathbf{x}}$ is given in (4) for completeness

$$\hat{\mathbf{x}} = \mathbf{C_x}(\mathbf{C_x} + \mathbf{C_n})^{-1}\mathbf{y}. \tag{4}$$

The covariance of the error of a Wiener estimate of $\mathbf{x}$ given $\mathbf{y}$, $\mathbf{C_e}$ is shown in (5)

$$\begin{aligned} \mathbf{C_e} &= E[(\mathbf{x} - \hat{\mathbf{x}})(\mathbf{x} - \hat{\mathbf{x}})^T] \\ &= \mathbf{C_x}(\mathbf{C_x} + \mathbf{C_n})^{-1}\mathbf{C_n}. \end{aligned} \tag{5}$$

The variance of the error for each variable is then given by the leading diagonal elements of $\mathbf{C_e}$

$$\sigma_e^2 = \frac{\sigma_x^2 \sigma_n^2 \left[(\sigma_x^2 + \sigma_n^2) - (\rho_x^2 \sigma_x^2 + \rho_n^2 \sigma_n^2) \right]}{(\sigma_x^2 + \sigma_n^2)^2 - (\rho_x \sigma_x^2 + \rho_n \sigma_n^2)^2}. \tag{6}$$

To analyze the behavior of σ_e^2, we take the derivative of (6) with respect to the signal correlation coefficient and simplify to obtain the expression in (7)

$$\frac{d(\sigma_e^2)}{d\rho_x} = \frac{2\sigma_x^4 \sigma_n^4}{\left[(\sigma_x^2 + \sigma_n^2)^2 - (\rho_x \sigma_x^2 + \rho_n \sigma_n^2)^2 \right]^2} \\ \times (\rho_x - \rho_n) \left[\rho_n (\rho_x \sigma_x^2 + \rho_n \sigma_n^2) - (\sigma_x^2 + \sigma_n^2) \right]. \tag{7}$$

The first product term in (7) is positive for all values of ρ_x, so the roots of (7) are determined by the final two product terms. Given this, (7) has the roots in (8) and (9)

$$\rho_x = \rho_n \tag{8}$$

$$\rho_x = \frac{1}{\rho_n} + \frac{\sigma_n^2}{\sigma_x^2} \left(\frac{1}{\rho_n} - \rho_n \right). \tag{9}$$

The first root lies in the interval $\rho_x \in (-1, 1)$. In (9), if it exists, either ρ_n is positive and the root is greater than one or ρ_n is negative and the root is less than minus one. Hence, the second root lies in $\rho_x \in (\infty, -1] \cup [1, \infty)$. These are the stationary points of σ_e^2 as a function of ρ_x, i.e., where the derivative is zero.

Since there is a single root of $(d(\sigma_e^2))/(d\rho_x)$ on the interval $\rho_x \in (-1, 1)$, we can determine the concavity of the error variance from the values of $(d(\sigma_e^2))/(d\rho_x)$ at $\rho_x = -1$ and $\rho_x = 1$.

Firstly we consider the estimation error variance gradient when $\rho_x = -1$

$$\frac{d(\sigma_e^2)}{d\rho_x}\bigg|_{\rho_x = -1} = \frac{2\sigma_x^4 \sigma_n^4}{\left[(\sigma_x^2 + \sigma_n^2)^2 - (\sigma_x^2 - \rho_n \sigma_n^2)^2 \right]^2} \\ \times (1 + \rho_n) \left[\sigma_x^2(1 + \rho_n) + \sigma_n^2 (1 - \rho_n^2) \right]. \tag{10}$$

By inspection, we see the expression in (10) is positive for all $\rho_n \in (-1, 1)$. Equation (11) gives the gradient when $\rho_x = 1$

$$\frac{d(\sigma_e^2)}{d\rho_x}\bigg|_{\rho_x = 1} = \frac{-2\sigma_x^4 \sigma_n^4}{\left[(\sigma_x^2 + \sigma_n^2)^2 - (\sigma_x^2 + \rho_n \sigma_n^2)^2 \right]^2} \\ \times (1 - \rho_n) \left[\sigma_x^2(1 - \rho_n) + \sigma_n^2 (1 - \rho_n^2) \right]. \tag{11}$$

The expression in (11) is negative for all $\rho_n \in (-1, 1)$. Therefore, σ_e^2 is concave for all $\rho_x \in [-1, 1]$ with a local maximum at $\rho_x = \rho_n$. This accords with the intuition that for the lowest estimation error the signal statistics should be as different as possible from those of the noise.

A consequence of this result is that if the noise correlation is closer to zero than that of the signal, increased signal correlation magnitude results in a lower estimation error. Note that this also implies that image restoration techniques using interscale phase to gain increased signal correlation may not be as effective if the noise present is coloured such that the coefficients of its wavelet domain representation are more correlated.

IV. DEROTATED COMPLEX WAVELET COEFFICIENTS

The constancy of the phase gradient relationship between wavelet scales demonstrated in Section II-B combined with the result of Section III motivates the use of coefficients whose phase has been "derotated" by twice the phase of their interpolated parent coefficient. In the presence of a multiscale feature, the phases of the derotated coefficients should be approximately aligned and, therefore, highly correlated. This correlation can then be used to provide improved signal estimation performance at these image features.

In both [5] and [6], the interscale phase relationships are captured using the modified product of coefficients at adjacent scales shown in (12), where x is a wavelet coefficient at a given scale and orientation, x_p is the corresponding parent coefficient at the next coarser scale and r is the product coefficient. $\angle(r)$ denotes the phase of r

$$\begin{aligned} |r| &= |x||x_p| \\ \angle(r) &= \angle(x) - 2\angle(x_p). \end{aligned} \tag{12}$$

However, in an image estimation context, avoidance of non-linearity is important for mathematical tractability so that the new representation can be readily used in an efficient estimation algorithm. For this reason we propose the use of a coefficient similar to that in (12) but with the magnitude of the child

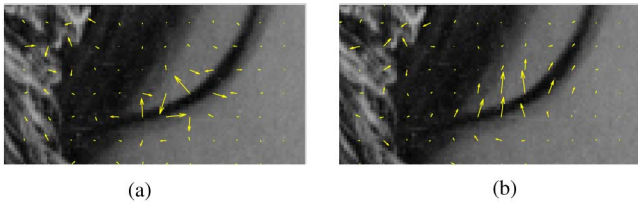Fig. 3.   Locations of overlay examples in Figs. 4 and 5.

Fig. 4.   DT-CWT and derotated coefficients at level 3, direction 1 (15°) in section 1 of the *Lena* image. (a) DT-CWT coefficients. (b) Derotated coefficients.

preserved. Equation (13) defines the new derotated coefficient, w

$$|w| = |x|$$
$$\angle(w) = \angle(x) - 2\angle(x_p). \qquad (13)$$

Analysis of this derotated coefficient via the DT-CWT filter banks is not straight-forward. However, analytical insight into the interscale phase relationships of the DT-CWT can be gained by considering the DT-CWT as a discrete approximation to the continuous Cauchy wavelet. An analysis along these lines is included in Appendix A and reveals the quadrature nature of the phases of derotated coefficients near edges compared to those near ridge features.

A. Derotated Coefficients in Two Dimensions

We now look at some examples of derotated coefficients in 2-D and consider their use in estimation algorithms. Figs. 4 and 5 contain examples of DT-CWT and derotated coefficients overlayed on part of the *Lena* image. Fig. 3 shows the original image and the locations of the examples. As we would expect, derotated coefficients are seen to align at edge and ridge features. Note that we are only considering features aligned with the orientation of the stated subband. Features with other orientations will not excite the coefficients' magnitudes. Note that for derotated coefficients within the same subband there is a 90 degree phase difference between the vectors near edges relative to those near ridges. See Appendix A for an explanation of this in 1-D.

Unfortunately, phase alignment does not guarantee increased correlation. Complex wavelet coefficients are a bandpass signal and will, therefore, rotate with an average rate proportional to the "center frequency" of the subband's spectrum. This rotation can have the appearance of a lack of correlation. However,
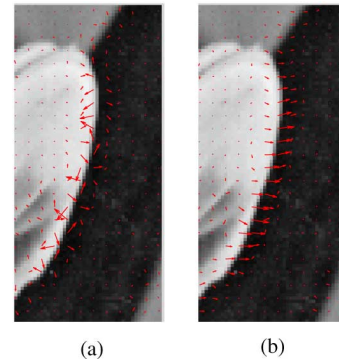

Fig. 5.   DT-CWT and derotated coefficients at level 2, direction 3 (75°) in section 2 of the *Lena* image. (a) DT-CWT coefficients. (b) Derotated coefficients.

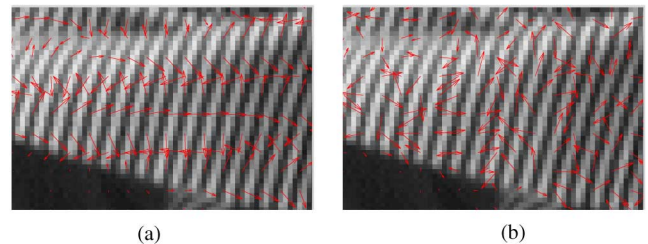Fig. 6.   Location of overlay example in Fig. 7.

Fig. 7.   DT-CWT and derotated coefficients at level 2, direction 3 (75°) in the *Barbara* image. (a) DT-CWT coefficients. (b) Derotated coefficients.

covariance information can adequately describe a linear phase gradient across coefficients. To determine how the derotation operation contributes to increased correlation we need to examine the correlation behavior of the two types of coefficient in greater detail. This is done in Section V.

B. Limitations of Derotated Coefficients

We should also consider the limitations of image modeling using derotated coefficients and the implications this has for their use in image estimation algorithms. Image features which are not multiscale are not suited to representation using derotated wavelet coefficients. Certain features, in particular areas of regular texture, tend to be more suited to representation using standard wavelet coefficients. Fig. 7 shows standard and derotated DT-CWT coefficients for part of the *Barbara* image shown in Fig. 6. The DT-CWT coefficients show significant correlation between neighboring coefficients whereas the derotated coefficients show neither alignment nor constant rotation across the vectors and have little correlation in these regions.
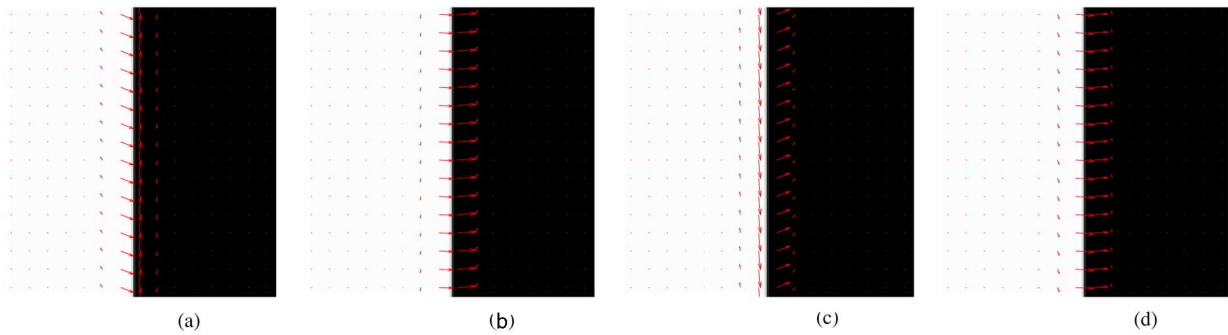
Fig. 8. DTCWT and derotated coefficients for straight edges at different offsets. (a) DTCWT coefficients—offset 1. (b) Derotated coefficients—offset 1. (c) DTCWT coefficients—offset 2. (d) Derotated coefficients—offset 2.

This has important implications for the use of derotated coefficients in image estimation algorithms. Derotated coefficients are not appropriate for modeling all feature types and restoration algorithms using them will need to have a mechanism for switching to other modeling methods for neighborhoods of coefficients without a dominant edge or ridge feature. In [1], this is achieved using a Bayesian model selection framework.

V. ANALYSIS OF DT-CWT AND DEROTATED COEFFICIENT CORRELATIONS

As mentioned previously, the phase alignment illustrated in Section IV-A does not guarantee increased correlation (applying a linear phase gradient across a set of coefficients will change their alignment but will not decrease the level of correlation between them). To apply the result of Section III-A to image estimation it is necessary to show that derotated coefficients have more consistent phase differences between coefficients, and, therefore, increased correlation at discontinuities compared to DT-CWT coefficients. It is also useful to know in which situations modeling using derotated coefficients is likely to offer the most improvement. Therefore, we now compare covariance information of derotated coefficients at discontinuities to that of standard DT-CWT coefficients. It turns out there are three mechanisms by which derotated coefficients provide an improved description of image discontinuities:

1) improved correlation along discontinuities;
2) improved correlation across discontinuities;
3) improved correlation across scale at edge features.

To begin, we examine the behavior of DT-CWT coefficients at discontinuities as a reference point to see what is gained by using derotated coefficients. This is done in Section V-A before covering the properties listed above in Sections V-B, V-C, and V-D. In all cases, it is assumed the discontinuity is approximately aligned with the subband's direction (i.e., within ±15 degrees). If this is not the case, the coefficients' magnitudes will be small.

Display of Covariance Information: To illustrate the complex covariance information for a neighborhood of coefficients, we display the cross correlation of a central coefficient with its neighbors using vectors with a circle at the base positioned at the location of the neighbor. The cross correlation with the parent coefficient is also displayed to the right. For the purpose of clear illustration we use only the complex covariance information for all DT-CWT and derotated coefficients.

A. Shift Invariance of Phase Differences: Both Types of Coefficient

First, we will consider the relationship between coefficients in the direction approximately perpendicular to the edge. We can explain the behavior of the phase of DT-CWT and derotated coefficients in 2-D in terms of the 1-D analysis as follows. The DT-CWT can be implemented using separable filters. For each subband, the decomposition can be expressed as a series of (real) 2-D low-pass filtering operations followed by a lowpass filtering in one direction and highpass in the other direction (near-horizontal and near-vertical subbands) or high-pass filtering in both dimensions (diagonal subbands). Thus, in the direction perpendicular to the discontinuity, the phase of the coefficients in 2-D rotate across the filtered discontinuity in a similar manner to the 1-D case.

Fig. 8 shows standard DT-CWT coefficients and derotated coefficients for a vertical edge at two offsets. The vectors have rotated as a result of the edge's shift. However, the phase differences between coefficients across the edge are preserved by the linearity of the step response illustrated in Fig. 1. The phase of the DT-CWT coefficients is not shift invariant but the phase differences between adjacent coefficients across the edge are. Both the phases of derotated coefficients and consequently their phase differences are shift invariant at the edge.

However, only phase differences between coefficients are relevant in determining covariance information. For both DT-CWT and derotated coefficients within a given subband, the covariance relationships for an edge at a particular orientation are independent of the exact position of the edge (note that the same is not true for the relationship with the parent coefficient). This is illustrated in Fig. 9, which shows the covariance information for the edges in Fig. 8. The covariance information within the same subband for the edge at offset 1 in Fig. 8(a) and (b) is very close to that for offset two shown in Figs. 8(c) and (d) for both DT-CWT and derotated coefficients.

B. Improved Correlation Along Discontinuities

Now consider Fig. 10, where the edge has been rotated clockwise by 30 degrees. The rotation causes the position of the DT-CWT coefficients relative to the edge to change along the edge. The phase differences across the edge remain invariant to the positional change caused by the rotation as explained
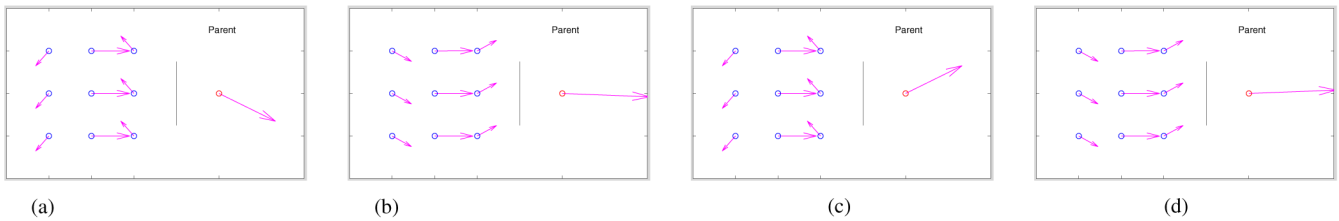
(a) (b) (c) (d)

Fig. 9. Complex covariance information for DT-CWT and derotated coefficients for edges at different offsets. The vector to the right corresponds to the cross correlation with the parent coefficient. (a) Covariance information for DT-CWT coefficients—offset 1. (b) Covariance information for derotated coefficients—offset 1. (c) Covariance information for DT-CWT coefficients—offset 2. (d) Covariance information for derotated coefficients—offset 2.
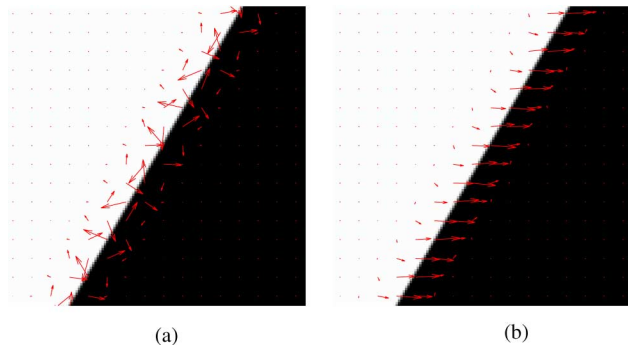

(a) (b)

Fig. 10. DTCWT and derotated coefficients for an edge at an angle. (a) DTCWT coefficients. (b) Derotated coefficients.
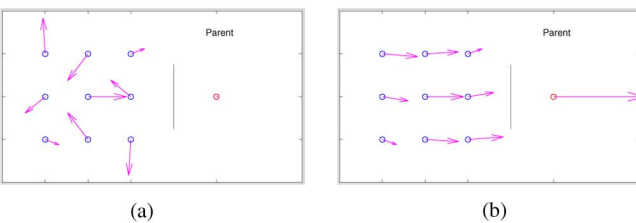

(a) (b)

Fig. 11. Covariance information for the edge at a different orientation in Fig. 10. The vector to the right corresponds to the cross correlation with the parent coefficient. (a) Covariance information for DT-CWT coefficients. (b) Covariance information for derotated coefficients.
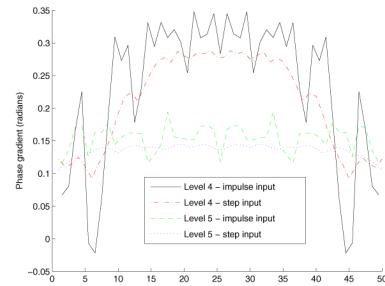

Fig. 12. Phase gradient of DT-CWT step and impulse response. The horizontal axis gives the relative position of the input in terms of the spatial domain sample rate.
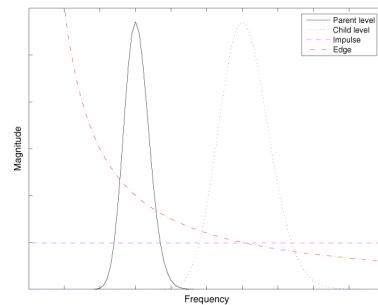

Fig. 13. Magnitude spectra of discontinuities and a bandpass signal.

above. However, there is now a phase change along the edge due to its rotation.

The change in this rate of rotation with the angle of the edge is approximately 135 degrees of coefficient phase rotation per 30 degrees (the angular support of each subband) of edge rotation. In contrast, the derotated coefficients' phases are invariant to the rotation of the edge, provided that its orientation is approximately aligned with that of the subband. This is illustrated by Fig. 11 showing the covariance information for the edge in Fig. 10. For DT-CWT coefficients, the covariance relationships in the direction approximately aligned with the edge are different from those for the vertical edges in Fig. 9 (by about 135 degrees). However, the derotated coefficient covariance information for the rotated edge in Fig. 10 is very similar to that for the vertical edge in Fig. 9.

Covariance information for derotated coefficients at discontinuities is more constant than for DT-CWT coefficients because the relationships between coefficients along the edge are more stable for different orientations of the discontinuity. This

means that, relative to derotated coefficients, the covariance information of wavelet coefficients for an edge at a given angle is sub-optimal in describing the behavior of coefficients for edges at other angles within the same angular support of the subband.

C. Improved Correlation Across Discontinuities

We now address the consistency of phase differences in the direction perpendicular to the edge or ridge. Because the magnitude of wavelet coefficients decreases rapidly in the direction perpendicular to the discontinuity, we are primarily concerned with the coefficients within a single sample space of the edge in the direction perpendicular to the discontinuity.

Fig. 12 shows the phase gradients for the impulse and step responses of the DT-CWT at levels 4 and 5 in 1-D. This is the first order derivative of the phase responses in Figs. 1 and 2. The plots are noisy relative to Figs. 1 and 2 because high frequencies have been boosted through differentiation. The gradient becomes smoother if longer q-shift filters are used in the DT-CWT. Nevertheless, the approximately constant gradient means the phase response is nearly linear over a distance up to about one sample either side of the discontinuity, although the
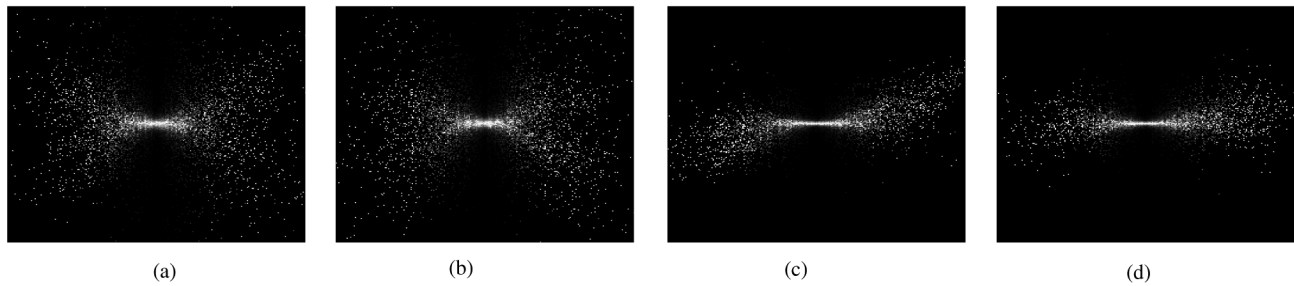
Fig. 14. Conditional histogram of real and imaginary parts of DT-CWT and derotated coefficients at adjacent scales. The horizontal axis corresponds to the child and the vertical axis to the parent coefficient. (a) DTCWT coefficients—real parts. (b) DTCWT coefficients—imaginary parts. (c) Derotated coefficients—real parts (corresponding to edge features). (d) Derotated coefficients—imaginary parts (corresponding to ridge features).

response is less linear for impulse features than for edges. Standard DT-CWT coefficients will rotate across the edge or ridge at a rate that is approximately constant irrespective of the exact position of the feature. However, Fig. 12 shows that this rate differs by about 10% depending on whether the feature is an edge or ridge.

A spectral explanation of this phenomenon is as follows. A forward DT-CWT transform can be considered to be a complex bandpass filtering operation with negative frequencies suppressed followed by decimation. Fig. 13 shows an illustrative diagram of the frequency spectrum of a particular subband before decimation in 1-D. Also drawn are the spectrum of the parent level subband, a flat spectrum and a $(1/f)$ spectrum, the latter two corresponding to impulse and edge features respectively.

Complex wavelet coefficients are a bandpass signal and will, therefore, rotate with an average rate that scales proportionally with the frequency of the passband. The filtering operation, corresponding to multiplication of the spectra in Fig. 13, will result in a higher average rate of rotation for the impulse than the edge feature. However, provided that a discontinuity at a given level has a similarly shaped spectrum over the parent subband, as is the case for the impulse and step spectra in Fig. 13, the phase differences between derotated coefficients will be close to zero across the feature.

At level 4 the higher rotation rate of coefficients near an impulse results in the phase difference between adjacent DT-CWT coefficients at an impulse being at most about 40 degrees more than that between coefficients at an edge, so the effect is less significant than the other effects discussed in this section.

D. Improved Correlation Across Scale at Edge Features

We see in Fig. 9, and especially in Fig. 11, that the parent coefficient correlation magnitude for DT-CWT coefficients is significantly less than that for derotated coefficients. DT-CWT coefficients generally display very little first-order correlation with their parent coefficient. This is a result of the differing phase gradients at each scale as illustrated in Fig. 2.

This lack of correlation was noted in [12] and is illustrated in Fig. 14(a) and (b), which show the conditional histogram of the real and imaginary parts of wavelet coefficients at two adjacent scales. A single directional subband at level 2 for various transposition and reflections of the *Peppers* image is used to generate the histograms. Fig. 14(c) and (d) shows the same histograms for the corresponding derotated coefficients. In this

case, the real parts of the coefficients correspond to edge features and the imaginary parts to ridge features.

Fig. 14(c) shows significant correlation between the real parts of derotated coefficients at adjacent scales. Derotated coefficients have good correlation with their parent at edges, due to their invariance to the exact position of the discontinuity, their consistent relationship with feature type at each level and because edges are commonly scale invariant across a number of scales. Note that the statistics in Fig. 14(c) are generated using the entire image containing a range of features in addition to multiscale edges, which contribute to the parts of the bow tie displaying less correlation. Any correlation between the imaginary parts in Fig. 14(d) is much less significant. The difference is that a ridge feature of a given width has an inherent scale, whereas an edge is scale invariant across all scales. A ridge at one scale acts more like two separate edges at a finer scales where its width becomes significant.

E. Summary of Derotated Coefficient Analysis

The preceding sections show that the phase shift invariance displayed by derotated coefficients means that covariance relationships between derotated coefficients are stronger than those between standard wavelet coefficients at structural image features. By extending the logic developed for the two variable wiener filtering case in Section III we conclude that provided the wavelet domain representation of the noise present is less correlated than that of the image, correlation (Wiener) based estimation of derotated coefficients will be more accurate than standard wavelet coefficients at image discontinuities.

Derotated coefficients will have the most impact in describing features at different angles including curving features. If all discontinuities are straight and in the same direction there will be reduced benefit. The use of derotated coefficients also means a parent coefficient makes a more useful contribution to predicting the child coefficient.

VI. Conclusion

A method for defining the statistics of natural images has been presented and analyzed. The method derotates complex wavelet coefficients by twice the phase of the parent coefficient to create a new "derotated" coefficient. This is a more linear representation than that used previously in [5] and [6] allowing the use of the coefficient in covariance based image estimation

algorithms. Compared to standard wavelet coefficients, derotated coefficients are more invariant to curvature and rotations of edge and ridge features and display increased correlation near these features. This allows improved correlation based signal estimation in these areas. This is demonstrated using a simple Wiener filtering example in [11]. The use of derotated coefficients in a state-of-the-art denoising algorithm is demonstrated in [1].

APPENDIX A
CAUCHY WAVELET ANALYSIS

In this Appendix, an analysis of derotated coefficients is performed by considering the DT-CWT as a discrete approximation to the continuous Cauchy Wavelet. This comparison was previously made by Romberg *et al.* in [8] to illustrate the interscale relationship of wavelet coefficient phases at edges. This analysis has been adapted to provide a theoretical background on the quadrature nature of the phase of derotated coefficients near edges and ridges. A similar analysis can be performed using a lowpass function modulated by a complex exponential. An analysis for such continuous wavelets (not derotated) is given in [7].

Equation (14) gives a generic form of the Cauchy wavelet including parameters ξ and A to control the phase and amplitude of the complex function

$$\psi(t) = A e^{i\xi} \left(1 - i\frac{t}{c} \right)^{-\alpha}. \tag{14}$$

The dilated and shifted versions of ψ are expressed using the notation in (15)

$$\psi_{v,u}(t) = \frac{1}{\sqrt{v}} \psi \left(\frac{t-u}{v} \right). \tag{15}$$

The real parameters $A, \xi, c,$ and α can be chosen to achieve a good approximation to the DT-CWT impulse response near the center of the main support of the wavelet function, the region with which we are primarily concerned. Fig. 15 shows the approximation at level 5 in 1-D for the parameter values in Table I.

We now examine the interscale phase relationships of the Cauchy wavelet analytically. The approximation to the DT-CWT in 1-D at level l and spatial location k is given in (16)

$$d_{l,k}(t) = \psi_{2^l,k}(t)$$
$$= 2^{-\frac{l}{2}} A e^{i\xi} \left(1 - i\frac{t-k}{2^l c} \right)^{-\alpha}. \tag{16}$$

This function has a phase ϕ, given in (17)

$$\phi_{l,k}(t) = \angle d_{l,k}(t)$$
$$= \xi - \alpha \tan^{-1} \left(-\frac{t-k}{2^l c} \right)$$
$$\approx \xi + \alpha \frac{t-k}{2^l c}. \tag{17}$$
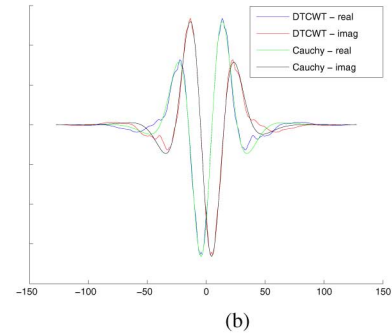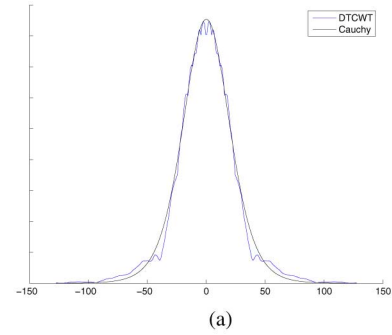

(a)

(b)

Fig. 15. Comparison of the Cauchy Wavelet and combined DT-CWT decomposition filter at level 5. The scale of the horizontal axis is that of the input in the spatial domain. Values for the parameters α, c, A, and ξ are given in Table I. (a) Magnitude response at level 3. (b) Impulse response at level 3.

TABLE I
PARAMETER VALUES USED IN CAUCHY WAVELET APPROXIMATION
TO DT-CWT IMPULSE RESPONSE IN FIG. 15

Parameter	Value
α	9.25
c	1.81
A	1.3
ξ	-0.75π

The final line of (17) follows if $|t - k|$ is small, i.e., near the center of the support of the wavelet function. Hence, derotated coefficients near an impulse have the phase approximation in (18)

$$\angle w_{l,k}(t) \approx \phi_{l,k}(t) - 2\phi_{l+1,k}(t)$$
$$= -\xi. \tag{18}$$

This phase is independent of t and k demonstrating how the multiscale nature of the impulse results in derotated coefficients whose phases are invariant to the exact location of the feature.

We now consider the step response, s and the corresponding phase response η

$$s_{l,k}(t) = \int_{-\infty}^{t} \psi_{2^l,k}(a) \, da$$
$$= \frac{i2^{\frac{l}{2}} c A e^{i\xi}}{-\alpha + 1} \left(1 - i\frac{t-k}{2^l c} \right)^{-\alpha+1}. \tag{19}$$

This has a phase given in (20)

$$
\begin{aligned}
\eta_{l,k}(t) &= \angle s_{l,k}(t) \\
&= -\frac{\pi}{2} + \xi - (\alpha - 1)\tan^{-1}\left(-\frac{(t-k)}{2^l c}\right) \\
&\approx -\frac{\pi}{2} + \xi + \frac{(\alpha - 1)(t-k)}{2^l c}.
\end{aligned} \tag{20}
$$

The derotated coefficients corresponding to the step response $s_{l,k}(t)$ have phases as described in (21)

$$
\begin{aligned}
\angle w_{l,k}(t) &\approx \eta_{l,k}(t) - 2\eta_{l+1,k}(t) \\
&= \frac{\pi}{2} - \xi.
\end{aligned} \tag{21}
$$

The phase in (21) is also invariant to the exact position of the edge feature and comparison with (18) illustrates the quadrature nature of the phases of derotated coefficients near edges and those near ridge features.

REFERENCES

[1] M. A. Miller and N. G. Kingsbury, "Image denoising using derotated complex wavelet coefficients," *IEEE Trans. Image Process.*, vol. 17, no. 9, pp. 1500–1511, Sep. 2008.

[2] J. Portilla, V. Strela, M. J. Wainwright, and E. P. Simoncelli, "Image denoising using Gaussian scale mixtures in the wavelet domain," *IEEE Trans. Image Process.*, vol. 12, no. 11, pp. 1338–1351, Nov. 2003.

[3] N. G. Kingsbury, "Complex wavelets for shift invariant analysis and filtering of signals," *J. App. Comput. Harmon. Anal.*, vol. 10, no. 3, pp. 234–253, May 2001.

[4] I. Selesnick, R. Baraniuk, and N. Kingsbury, "The dual-tree complex wavelet transform," *IEEE Signal Process. Mag.*, vol. 22, no. 6, pp. 123–151, Nov. 2005.

[5] J. Portilla and E. P. Simoncelli, "A parametric texture model based on joint statistics of complex wavelet coefficients," *Int. J. Comput. Vis.*, vol. 40, no. 1, pp. 49–71, Dec. 2000.

[6] R. Anderson, N. Kingsbury, and J. Fauqueur, "Coarse level object recognition using interlevel products of complex wavelets," in *Proc. IEEE Int. Conf. Image Processing*, Sep. 2005, pp. 745–748.

[7] Z. Wang and E. P. Simoncelli, "Local phase coherence and the perception of blur," *Adv. Neural Inf. Process.*, vol. 16, pp. 786–792, May 2004.

[8] J. K. Romberg, H. Choi, and R. G. Baraniuk, "Multiscale edge grammars for complex wavelet transforms," in *Proc. IEEE Int. Conf. Image Processing*, Thessaloniki, Greece, Oct. 2001, pp. 614–617.

[9] P. Kovesi, "Image features from phase congruency," *Videre: J. Comput. Vis. Res.*, vol. 1, no. 3, pp. 2–26, May 1999.

[10] P. Kovesi, "Edges are not just steps," in *Proc. 5th Asian Conf. Computer Vision*, Mebourne, Australia, Jan. 2002, pp. 822–827.

[11] M. A. Miller and N. G. Kingsbury, "Statistical image modelling using interscale phase relationships of complex wavelet coefficients," in *Proc. IEEE Int. Conf. Acoustics, Speech, and Signal Processing*, Toulouse, France, May 2006, vol. 2, pp. 789–792.

[12] M. J. Wainwright and E. P. Simoncelli, "Scale mixtures of Gaussians and the statistics of natural images," *Adv. Neural Inf. Process.*, vol. 12, pp. 855–861, 2000.

Mark Miller (M'06) received an honors degree in electrical and electronic engineering from the University of Canterbury, New Zealand, in 2002, and the Ph.D. degree in multiscale image processing from Trinity College, Cambridge, U.K.

He worked as a Research Assistant at the University of Canterbury developing a synthetic aperture sonar motion correction algorithm before completing the Ph.D. degree.

Nick Kingsbury (M'86) received the honors degree and the Ph.D. degree in electrical engineering from the University of Cambridge, Cambridge, U.K., in 1970 and 1974, respectively.

From 1973 to 1983, he was a Design Engineer and, subsequently, a Group Leader with Marconi Space and Defence Systems, Portsmouth, U.K., specializing in digital signal processing and coding as applied to speech coders, spread spectrum satcomms, and advanced radio systems. Since 1983, he has been a Lecturer in communications systems and image processing at the University of Cambridge and a Fellow of Trinity College, Cambridge. He was appointed to a readership in signal processing in 2000 and to Professor of signal processing in 2007. He is now Head of the Signal Processing Group, Department of Engineering, Cambridge University.